

Chromomagnetic condensation and perturbative confinement induced by imaginary rotation in SU(2) Yang-Mills Theory

Lei Zhang,^{1,*} Kun Xu,^{2,†} and Mei Huang^{3,‡}

¹*School of Physical Sciences, University of Chinese Academy of Sciences, Beijing 101408, China*

²*School of Physics, Beijing Institute of Technology, Beijing, 100049, P.R. China*

³*School of Nuclear Science and Technology, University of Chinese Academy of Sciences, Beijing, 101408, P.R. China*

(Dated: February 6, 2026)

We perturbatively investigate the rotation effect on the Polyakov loop potential in SU(2) gauge theory within a chromomagnetic background. It is observed that the imaginary rotation spontaneously induces both confinement and chromomagnetic condensation at high temperatures, thereby provides a perturbative window to explore non-perturbative dynamics. Compared to the case without including the induced chromomagnetic field, the perturbative confinement transition becomes first-order, with a temperature-dependent phase boundary that asymptotically approaches $\tilde{\Omega}_c = \pi/\sqrt{3}$ at high temperatures. This leads to a significantly enriched $\tilde{\Omega}$ - T phase diagram characterized by an expanded deconfined region. For real angular velocities, we find that the chromomagnetic condensate decreases with increasing rotation, and that the coupling between rotation, spin, and the chromomagnetic background leads to a cusp in the Polyakov loop potential, suggesting that the underlying dynamics could be more intricate.

I. INTRODUCTION

In $SU(N)$ theories, the negative sign of the β function in the renormalization group flow, manifesting asymptotic freedom at ultraviolet(UV). In the infrared, the coupling grows without bound within perturbation theory, signaling the onset of a strongly coupled confining phase where perturbative methods fail. The non-perturbative effects in $SU(N)$ theories—confinement and chiral symmetry breaking—have long been central themes in the study of strong interactions. The most significant non-perturbative property is the existence of a deconfinement phase transition at finite temperature, investigated through non-perturbative methods such as semi-classical contributions [1–4], lattice regularization [5–7], functional renormalization group [8], Dyson-Schwinger equations [9], and phenomenological effective models [10]. These approaches have yielded many crucial insights.

In the heavy quark limit, the order parameter describing the deconfinement phase transition is the Polyakov loop in the fundamental representation, which is the trace of a Wilson line winding around the compactified Euclidean time direction. The modulus (or magnitude) of the Polyakov loop $|L|$ for simplicity denoted as $|L|$ represents the effect of a static color source at finite temperature: its expectation value gives the free energy required to insert an infinitely heavy, static test charge in the fundamental representation into a thermal medium of gluons, i.e.,

$$|L| \propto e^{-\beta F_q}, \quad |L| \in [0, 1]. \quad (1)$$

$SU(N)$ gauge theories possess a $\mathbb{Z}(N)$ center symmetry. This symmetry is intimately connected to the be-

havior of the Polyakov loop under such transformations, making it the order parameter for this symmetry. Thus, the Polyakov loop tightly links the physical phenomenon of confinement to the mathematical framework of center symmetry and its spontaneous breaking. In the confined phase: the free energy required to pull an isolated static quark from the vacuum is infinite, corresponding to $|L| = 0$, and the $\mathbb{Z}(N)$ symmetry is unbroken. In the deconfined phase: color charge can be screened by the thermal medium, allowing a single static quark to exist with finite free energy, corresponding to $|L| \neq 0$, and the $\mathbb{Z}(N)$ symmetry is spontaneously broken. The magnitude of $|L|$ directly reflects the strength of the screening.

As a key component of the QCD phase structure, the behavior of the deconfinement phase transition is indeed regulated by various external parameters. Examples include the inverse magnetic catalysis effect under external magnetic fields [11–13] and the search for the Critical End Point (CEP) at finite density [14–16]. In non-central relativistic heavy-ion collisions, a nuclear system is created with significant rotation and high temperature [17–20], where the vorticity ω of the created matter can be as large as 10^{22}s^{-1} . The effect of rotation ω has attracted widespread theoretical and experimental attention, becoming an important external parameter in quantum field theory research, alongside temperature, chemical potential, and magnetic field.

Rotation effects have been extensively studied in various systems including complex scalar fields [21–23], fermion fields [24–27], and vector fields [28, 29]. Such effects exist in diverse systems; for instance, heavy nuclei with spontaneously broken rotational symmetry can restore it under external rotation, generating rotational bands [30, 31]. In QCD, rotation leads to important phenomena such as the chiral vortical effect [32–35]. A fundamental inquiry then arises: how the QCD phase structure evolves under the influence of ω , particularly regarding the chiral phase transition [25, 26, 36–40]. Recently,

* Correspond to zhanglei231@mails.ucas.ac.cn

† Correspond to xukun@bit.edu.cn

‡ Correspond to huangmei@ucas.ac.cn

rotating gluonic systems and the deconfinement phase transition have garnered significant attention, stemming from the larger spin polarization of gluons and the dominance of soft gluons in the Quark-Gluon Plasma (QGP). The deconfinement phase transition in QCD under rotation has also drawn focus [41–51]. However, in rotating systems, challenges arise for lattice calculations from both the consistency between rotational effects and finite density effects [25, 26] and the fact that rotation makes the pure gauge action complex, introducing a new sign problem. Alternatively, performing lattice QCD simulations by introducing an imaginary angular velocity ($\Omega = -i\omega$) is feasible and has yielded many interesting results [42, 43, 45]. However, most model results contradict these findings.

As outlined above, research on the deconfinement phase transition is fundamentally based on non-perturbative methods. Perturbative calculations of the effective potential for L show that the $\mathbb{Z}(N)$ symmetry is broken at high temperatures, but cannot provide information about its restoration at low temperatures and its relation to confinement [5, 52, 53]. However, a recent calculation demonstrates that pure Yang-Mills (YM) theory at sufficiently large Ω undergoes a confinement phase transition even perturbatively at the rotation center $r = 0$. This implies that imaginary rotation Ω provides a unique framework to manifest non-perturbative physical results within the perturbative regime, which is quite intriguing in itself [54].

Notably, in previous studies, a constant chromomagnetic field – the Savvidy vacuum – as the simplest form of non-perturbative vacuum, allows for the analytical evaluation of the one-loop functional determinant [55–63]. Its perturbative prediction shows a non-trivial minimum at $H \neq 0$, indicating the existence of chromomagnetic condensation in the vacuum state of non-Abelian gauge theories. While lattice calculations have not found any long-range order for chromomagnetic condensation, the non-zero gluon condensate $\langle G_{\mu\nu}^a G^{a\mu\nu} \rangle$ implies its existence locally [7]. More crucially, the coupling of the Polyakov loop to a gauge field condensate exhibits complex interplay. Locally at the rotation center $r = 0$, a directed constant color-magnetic background, together with the spin-rotation coupling, modulates the single-particle spectrum, while the chromoelectric background ϕ acts as an imaginary chemical potential affecting statistical distribution. The interplay between these three factors may give rise to new minima, cusps, or imaginary components in the effective potential, ultimately leading to a more complex phase structure.

In this work, we derive the one-loop effective potential for pure SU(2) theory under rotation in the presence of chromoelectric and chromomagnetic background fields. We identify two components within the effective potential: one promotes chromomagnetic condensation and another suppresses it. In the perturbative regime, our results show strong suppression of chromomagnetic condensation. However, the inclusion of imaginary rotation

introduces a novel competitive relationship between these two potential components, leading to an explicit breaking of $\mathbb{Z}(2)$ symmetry. This causes significant changes in the region of perturbative confinement, the order of the phase transition, and the temperature dependence of the phase boundary. The adiabatic continuity from the perturbative confinement to the confined phase at low temperature might be affected along its path in the phase diagram, also suggesting that at larger imaginary rotations, the critical temperature for deconfinement in the non-perturbative regime may exhibit a non-monotonic dependence on the imaginary rotation. We also address subtleties in the analytical continuation from imaginary to real angular velocity by imposing a causality bound.

This paper is organized as follows. In Sec. II, we develop the formalism required for evaluating the one-loop effective potential. In Sec. III, we calculate the Polyakov loop potential at different temperatures, presenting the complex coupling phenomenon between the Polyakov loop and chromomagnetic condensation. We analyze the subtle competitive relationship between the chromomagnetic-favoring potential V_H and the chromomagnetic-suppressing potential $V_{\text{non}H}$ under imaginary rotation, predicting the order of the rotation-induced perturbative confinement phase transition and the temperature dependence of the phase boundary. In Sec. IV, we compute the impact of different imaginary rotations on the Polyakov loop potential and obtain the phase diagram for the perturbative confinement phase. In Sec. V, we investigate the effects of real rotation on chromomagnetic condensation and the Polyakov loop potential by imposing boundary conditions. We conclude and provide an outlook in Sec. VI.

II. POLYAKOV LOOP POTENTIAL WITH IMAGINARY ROTATION

In this section, we introduce the formalism necessary to evaluate the one-loop effective potential for SU(2) gauge bosons at finite temperature propagating in a special class of background field configurations.

The quadratic fluctuation action in the background field of the SU(2) Yang-Mills theory is given by:

$$\mathcal{L}_0 = -\frac{1}{2} \hat{Q}^+ \cdot \hat{Q}^- - ig Q_\mu^+ Q_\nu^- B^{\mu\nu} - \frac{1}{4} \tilde{Q}^3 \cdot \tilde{Q}^3 - \frac{1}{4} B \cdot B, \quad (2)$$

with

$$\hat{Q}_{\mu\nu}^+ = D_{[\mu} Q_{\nu]}^+, \quad \tilde{Q}_{\mu\nu}^3 = \partial_{[\mu} Q_{\nu]}^3, \quad B_{\mu\nu} = \partial_{[\mu} B_{\nu]}. \quad (3)$$

Here, B denotes the background field. It is convenient to identify the fields $Q^\pm = \frac{1}{\sqrt{2}} (Q^1 \pm iQ^2)$ and Q^3 as analogous to the W^\pm and Z^0 fields, carrying charges ± 1 and 0 , respectively. The neutral Z^0 particle behaves as a free field, while the W^\pm particles behave as charged, spin-1 particles propagating in an external field.

Traditionally, we choose the chromomagnetic field H to point along the z -direction, which is given by

$$B_\mu = \frac{H}{2}(0, y, -x, 0) = \frac{1}{2}H\epsilon_{0\mu\nu3}x_\nu. \quad (4)$$

Under the gauge condition $D_\mu Q^\mu = (\partial_\mu + igB_\mu)Q^\mu = 0$, the equation of motion (EOM) for Q^s ($s = \pm$) in the background field is obtained as

$$(\partial^2 + \frac{1}{4}gH^2\rho^2 - gH\hat{L}_z + 2sgH)Q^s = 0. \quad (5)$$

The eigenmodes (radial part labeled by (m, l, s)) are

$$\Phi_{\hat{m}}^{(l)}(\rho, \theta) = \sqrt{\frac{gH}{2\pi} \frac{\hat{m}!}{(|l| + \hat{m})!}} L_m^{(|l|)}(X) X^{|l|/2} e^{-\frac{1}{2}X} e^{il\theta}, \quad (6)$$

with the eigenvalues

$$E^2 = k_z^2 + (2m + 2s + 1)gH. \quad (7)$$

where $X = \frac{1}{2}gH\rho^2$ and $\hat{m} = m + (l - |l|)/2$. Subsequently, we simultaneously introduce a chromoelectric background field B_0 and rotation about the z -axis with angular velocity ω . According to reference [28], the Lagrangian of the system transforms as follows:

$$\partial_\mu \rightarrow \partial_\mu + \delta_{\mu 0}R_0, \quad B_\mu \rightarrow B_\mu + \delta_{\mu 0}B_0, \quad (8)$$

where the operator R_0 acts only on the spatial components of a vector field according to

$$R_0 A_i = -i\omega \hat{L}_z A_i + \omega \epsilon_{i3k} A_k. \quad (9)$$

Under this transformation, we find a remarkably simple modification to the EOM and the gauge condition:

$$\partial_0 \rightarrow \partial_0 + igB_0 - i\omega(\hat{L}_z - s). \quad (10)$$

This form reveals a striking symmetry of the chromomagnetic field within this rotating system. In an appropriate gauge, all explicit coupling terms between the rotation ω and the chromomagnetic field H in the EOM vanish. Consequently, the eigenmodes remain unchanged, while only the eigenvalues become

$$[E - gB_0 + (l - s)\omega]^2 = k_z^2 + (2m + 2s + 1)gH. \quad (11)$$

The detailed derivation is provided in Appendix A. It is noteworthy that the form of the chromomagnetic background field remains invariant under rotation, unlike the case of an external magnetic field that would be modified by rotation. As a vacuum state spontaneously chosen by the physical system, we find that such a configuration of the chromomagnetic field corresponds to a lower-energy state permitted in the rotating system. The Polyakov loop is specified by a constant B_0 field, given in the fundamental representation by

$$B_0 \rightarrow -i(g\beta)^{-1}\phi, \quad (12)$$

where $\phi \in [0, 2\pi]$. The trace of the background Polyakov loop is given by

$$L = \text{Tr } \mathcal{P} \exp \left(ig \int_0^\beta d\tau B_4(\vec{x}, \tau) \right) = 2 \cos(\phi/2). \quad (13)$$

Although the effective potential has a tachyonic instability with respect to long-wavelength fluctuations [57], subsequent studies have shown that, for the unstable modes, including the cubic and quartic terms in the fluctuations yields a real energy density, in agreement with the real part obtained from the quadratic approximation in earlier studies [64, 65]. Therefore, we can safely obtain the vacuum part and the finite-temperature part of one-loop effective potential:

$$V_0 = \frac{11(gH)^2}{48\pi^2} \ln \left(\frac{gH}{\Lambda^2} \right), \quad (14)$$

$$V_T = \frac{T}{S} \sum_{m=0}^{\infty} \sum_{s=\pm} \sum_{l=-m}^{N-m} \int_{-\infty}^{+\infty} \frac{dk_z}{2\pi} \ln \left| 1 - 2 \cos [\phi + (l - s)\tilde{\Omega}] e^{-\beta\omega_s} + e^{-2\beta\omega_s} \right|. \quad (15)$$

Here $\tilde{\Omega} = \beta\Omega$, and the background B_0 field and the imaginary angular velocity Ω shift the sum over Matsubara frequencies by a factor of $\phi/\beta + (l - s)\Omega$; Λ is a renormalization group-invariant parameter that sets the scale for the gauge theory. In above equation, S is the area of the xy -plane, N represents the degeneracy of the Landau level [25], and $\omega_s = \sqrt{k_z^2 + (2m + 2s + 1)gH}$ is the spectrum of the charged W^\pm particles in two polarization states within the field, $m \in \mathbb{N}$ is the Landau quantum number, and s denotes the spin orientation along ($s = 1$) or opposite ($s = -1$) the magnetic field direction (the $s = 0$ modes of the gauge field are cancelled by the contribution of the ghost field).

The local thermodynamic potential density $V_T(\vec{r})$ satisfies:

$$V_T = \frac{1}{V} \int d\rho d\theta dz V_T(\vec{r}), \quad (16)$$

yielding:

$$V_T(\vec{r}) = \sum_{s=\pm} \sum_{m=0}^{\infty} u(s, m, \vec{r}), \quad (17)$$

$$u(s, m, \vec{r}) = T \sum_{l=-m}^{N-m} |\Phi_{\hat{m}}^{(l)}(\rho, \theta)|^2 \int_{-\infty}^{+\infty} \frac{dk_z}{2\pi} \ln \left| 1 - 2 \cos [\phi + (l - s)\tilde{\Omega}] e^{-\beta\omega_s} + e^{-2\beta\omega_s} \right|. \quad (18)$$

In this work, we shall focus on the rotation center $r = 0$. Utilizing the property:

$$\lim_{\vec{r} \rightarrow 0} |\Phi_n^{(l)}(\rho, \theta)|^2 = \frac{gH}{2\pi} \delta_{l,0}, \quad (19)$$

we find that at $\vec{r} = 0$, the orbital angular momentum states are frozen, leaving only the spin states. The corresponding expressions are obtained as:

$$u(-, 0, \vec{0}) = \frac{gH}{2\beta\pi} \int_{-\infty}^{+\infty} \frac{dk}{2\pi} \ln \left| 1 - 2 \cos(\phi + \tilde{\Omega}) e^{-\beta\sqrt{k^2 - gH}} + e^{-2\beta\sqrt{k^2 - gH}} \right|, \quad (20)$$

$$u(-, 1, \vec{0}) = \frac{gH}{\beta\pi} \int_{-\infty}^{+\infty} \frac{dk}{2\pi} \operatorname{Re} \ln \left(1 - e^{-\beta\sqrt{k^2 + gH} + i(\phi + \tilde{\Omega})} \right), \quad (21)$$

$$V_{\text{nonH}} = \frac{gH}{\beta\pi} \sum_{m=1}^{\infty} \sum_{s=\pm} \int_{-\infty}^{+\infty} \frac{dk}{2\pi} \operatorname{Re} \ln \left(1 - e^{-\beta\omega + i[\phi - s\tilde{\Omega}]} \right), \quad (22)$$

where $\omega = \sqrt{k^2 + (2m+1)gH}$. Here, V_{nonH} represents the contribution from higher Landau levels:

$$V_{\text{nonH}} = \sum_{m=2}^{\infty} u(-, m, \vec{0}) + \sum_{m=0}^{\infty} u(+, m, \vec{0}). \quad (23)$$

It can be shown that in the limit $H \rightarrow 0$, only this part yields a non-zero contribution to the potential, reducing to the effective potential found in reference [54] (see Appendix C). Therefore, it is numerically impossible to achieve a perfectly vanishing H . To ensure convergence, the summation over Landau levels must be carried out up to an order of magnitude of approximately $O(H^{-1})$. In our calculation, we set a lower limit of the scaled variable

$\beta\sqrt{gH} = 0.01$, at which point V_{nonH} essentially coincides with the exact value, and the chromomagnetic field at this setting is regarded as vanishing. In the subsequent discussion, we will identify this as the chromomagnetic-suppressing potential.

Furthermore, the above expressions admit an alternative representation in series form. Using the series expansion $\ln(1 - z) = -\sum_{n=1}^{\infty} z^n/n$ for $|z| \leq 1$ and the following integral identities [63]:

$$K_1(n\beta m) = \frac{1}{2m} \int_{-\infty}^{+\infty} dk e^{-n\beta\sqrt{k^2 + m^2}}, \quad (24)$$

$$\lim_{\epsilon \rightarrow 0^+} \operatorname{Re} \int_0^{+\infty} \frac{dk}{2\pi} e^{-n\sqrt{k^2 - k_c^2 - i\epsilon}} = -\frac{k_c}{4} Y_1(nk_c), \quad (25)$$

we obtain the series expressions:

$$u(-, 0, \vec{0}) = \frac{(gH)^{\frac{3}{2}}}{\pi^2\beta} \sum_{n=1}^{\infty} \frac{1}{n} \frac{\pi}{2} Y_1(n\beta\sqrt{gH}) \cos n(\phi + \tilde{\Omega}), \quad (26)$$

$$u(-, 1, \vec{0}) = -\frac{(gH)^{\frac{3}{2}}}{\pi^2\beta} \sum_{n=1}^{\infty} \frac{1}{n} K_1(n\beta\sqrt{gH}) \cos n(\phi + \tilde{\Omega}), \quad (27)$$

$$V_{\text{nonH}} = -2 \frac{(gH)^{\frac{3}{2}}}{\pi^2\beta} \sum_{n=1}^{\infty} \sum_{m=0}^{\infty} \frac{1}{n} \sqrt{2m+3} K_1(n\beta\sqrt{gH(2m+3)}) \cos n\phi \cos n\tilde{\Omega}. \quad (28)$$

Numerical calculations indicate that the series representation for V_{nonH} converges faster, while the opposite is true for $u(-, 0, \vec{0})$. Consequently, in the final calculation of the total potential, we employ a hybrid approach, using the integral representation for some terms and the series representation for others:

$$\begin{aligned} V(\vec{r} = 0) &= \frac{11g^2H^2}{48\pi^2} \ln \left(\frac{gH}{\Lambda^2} \right) + \frac{gH}{2\pi\beta} \sum_{s=\pm} \int_{-\infty}^{+\infty} \frac{dk}{2\pi} \ln \left| 1 - 2 \cos(\phi + \tilde{\Omega}) e^{-\beta\sqrt{k^2 + sgH}} + e^{-2\beta\sqrt{k^2 + sgH}} \right| \\ &\quad - 2 \frac{(gH)^{\frac{3}{2}}}{\pi^2\beta} \sum_{n=1}^{\infty} \frac{1}{n} \cos n\phi \cos n\tilde{\Omega} \sum_{m=0}^{\infty} \sqrt{2m+3} K_1(n\beta\sqrt{(2m+3)gH}). \end{aligned} \quad (29)$$

As is evident, under the condition that $H \neq 0$ and $\tilde{\Omega} \neq 0$, the presence of the Lowest Landau Level (LLL) leads to a thermodynamic potential which no longer respects the symmetry $V(\phi) = V(2\pi - \phi)$. Consequently, the $\mathbb{Z}(2)$ center symmetry undergoes explicit breaking. This explicit breaking is likely to exert a non-trivial influence on the characteristics of the perturbative confinement phase

transition induced by Ω . In all subsequent calculations of the effective potential, we will adopt the dimensionless form $\beta^4 V$ for computation and analysis. The associated gap equations are given by

$$\frac{\partial V}{\partial H} = \frac{\partial V}{\partial \phi} = 0. \quad (30)$$

III. EFFECTS OF TEMPERATURE AND IMAGINARY ANGULAR VELOCITY

Within the chromomagnetic background field, we define the effective potential for the Polyakov loop as:

$$V(\phi) = V(\langle H \rangle, \phi), \quad (31)$$

where $\langle H \rangle$ satisfies:

$$\partial_H V(H, \phi) \Big|_{H=\langle H \rangle} = 0. \quad (32)$$

As demonstrated in reference [63], there exists a complex dependence between the chromomagnetic condensation H and the Polyakov loop ϕ . Notably, for $T < 0.2\Lambda$, the Savvidy model exhibits intriguing oscillations between confined and deconfined phases as the temperature varies. When $T > 0.2\Lambda$, this oscillatory behavior disappears. Within the temperature interval $\Lambda^{-1}T \in (0.20, 0.72)$, the minimum of $V(\phi)$ resides at the confining, non-trivial Polyakov loop value $\phi = \pi$. As the temperature exceeds the upper threshold, it discontinuously jumps to the deconfining, trivial Polyakov loop values $\phi = 0$ and 2π . We now investigate the evolution of the Polyakov loop potential with increasing T to observe this behavior with $\Omega = 0$.

Fig. 1 shows the evolution of the dimensionless Polyakov loop potential (scaled by T^4) in terms of ϕ with increasing temperature at $\Omega = 0$ and $r = 0$, alongside the corresponding scaled variable $\beta\sqrt{\langle gH \rangle}$. At any temperature, the potential is symmetric about $\phi = \pi$, reflecting the $\mathbb{Z}(2)$ center symmetry. The dependence of $\beta\sqrt{\langle gH \rangle}$ on ϕ reveals the intricate entanglement between chromomagnetic condensation and the Polyakov loop. At low temperatures, the Polyakov loop potential features two types of minima: shallow ones located at $\phi = 0, 2\pi$ and a sharp one at $\phi = \pi$. Thermal effects suppress the minimum at $\phi = \pi$. Upon reaching a certain threshold temperature, the global minimum discontinuously jumps to $\phi = 0, 2\pi$, and $\beta\sqrt{\langle gH \rangle}$ simultaneously jumps from π (which is determined by the LLL [63]) to 0. This suggests a first-order deconfinement phase transition. It is noteworthy, however, that lattice results have long established that the SU(2) deconfinement transition belongs to the three-dimensional Ising universality class [66], corresponding to a second-order transition. The discrepancy arises because our one-loop calculation is not applicable in the low-temperature, non-perturbative regime. In subsequent calculations, we set a lower temperature limit $T_{\text{pert}} = 10\Lambda$ to ensure reliability, treating the region $T < T_{\text{pert}}$ as the Strong Coupling Transition Region.

As shown in references [63], the contributions to the effective potential from both the LLL and the pure vacuum energy density each exhibit their minimum at a non-vanishing chromomagnetic field. leading us to identify

the chromomagnetic-favoring potential V_H :

$$V_H = \frac{11g^2H^2}{48\pi^2} \ln\left(\frac{gH}{\Lambda^2}\right) + \frac{gH}{2\pi\beta} \sum_{s=\pm} \int_{-\infty}^{+\infty} \frac{dk_z}{2\pi} \ln \left| 1 - 2 \cos(\phi + \tilde{\Omega}) e^{-\beta\sqrt{k_z^2 + sgH}} + e^{-2\beta\sqrt{k_z^2 + sgH}} \right|. \quad (33)$$

Calculations for the high-temperature part in Figure 1 reveal that chromomagnetic condensation is strongly suppressed at the minimum, effectively vanishing. This state persists in the region $T > T_{\text{pert}}$. A rough analysis based on the dimensionless vacuum energy (scaled by T^4) shows that thermal effects suppress chromomagnetic condensation, shifting the minimum of V_H towards smaller $\beta\sqrt{gH}$ and higher potential energy as temperature increases. Consequently, the overall potential tends to disfavor the generation of the scaled chromomagnetic condensation.

Figure 2 shows the chromomagnetic-favoring potential $V_H(H, \phi)$ and the chromomagnetic-suppressing potential $V_{\text{nonH}}(H, \phi)$ at $\Omega = 0$ and $T = 10\Lambda$. V_{nonH} is independent of temperature. The left panel clearly shows that the global minimum is located at $\phi = 0, 2\pi$ with $H \rightarrow 0$. V_{nonH} exhibits a suppressing effect on chromomagnetism: as H increases, $|V_{\text{nonH}}|$ becomes smaller, meaning the potential energy at $\phi = 0, 2\pi$ rises, bringing the potential contour closer to the $V = 0$ plane. According to Appendix C, we can analyze this roughly. V_{nonH} satisfies the expression:

$$V_{\text{nonH}} = \Delta x \sum_{n=1}^{\infty} f(x_n), \quad (34)$$

which represents an integral expression with step size $\Delta x = \beta^2 gH$, variable $x_n = n\beta^2 gH$, and integration interval $[0, +\infty)$, where the integrand f is monotonic and convergent in x . A larger step size leads to a smaller absolute value of the integral. The right panel shows that the minimum of V_H is located in the region with $\phi = 0, 2\pi$ and $H \neq 0$. However, this minimum is at a significantly higher energy level compared to V_{nonH} and holds no advantage. When the imaginary angular velocity is zero, the physical ground state in the perturbative regime is entirely dominated by V_{nonH} , and chromomagnetism is suppressed.

However, the situation changes as $\tilde{\Omega}$ increases, because the effect of the imaginary angular velocity on V_H and V_{nonH} is markedly different. Based on the overall symmetry of the potential:

$$V(H, \phi, \tilde{\Omega}) = V(H, 3\pi - \phi, \pi - \tilde{\Omega}), \quad (35)$$

our subsequent analysis of the imaginary angular velocity effect can be confined to the interval $\tilde{\Omega} \in [0, \pi/2]$. The physical minimum (H, ϕ) satisfies:

$$(H, \phi) \Big|_{\pi - \tilde{\Omega}} = (H, 3\pi - \phi) \Big|_{\tilde{\Omega}}. \quad (36)$$

First, from the expression for V_H , it is straightforward to see that the imaginary angular velocity shifts the entire

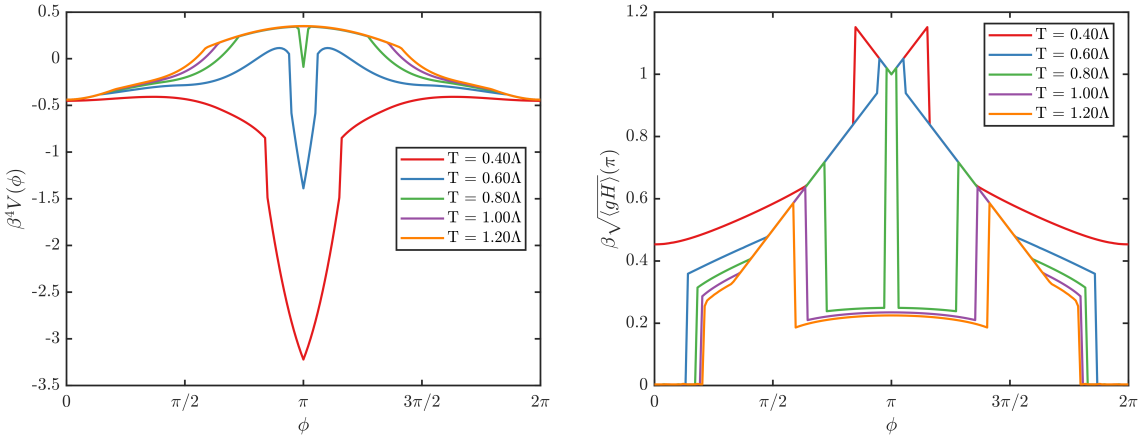


FIG. 1: Evolution of the dimensionless Polyakov loop potential $\beta^4 V$ (left) and the corresponding scaled variable $\beta\sqrt{gH}/\pi$ (right) as functions of ϕ at several temperatures, for $\Omega = 0$ and $r = 0$.

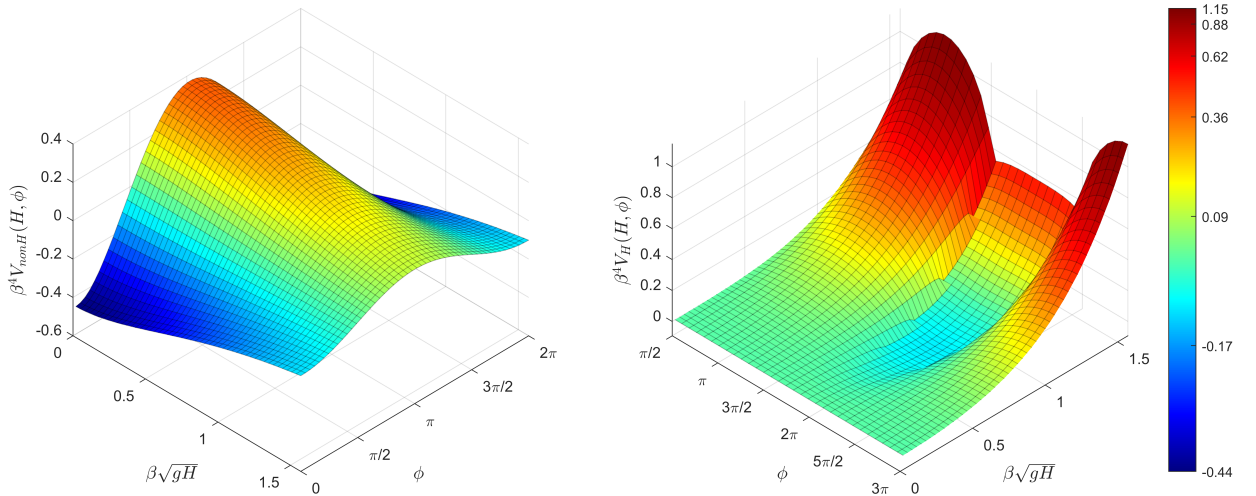


FIG. 2: Three-dimensional plots of the dimensionless potentials $\beta^4 V_{\text{nonH}}$ (left) and $\beta^4 V_H$ (right) as functions of ϕ and $\beta\sqrt{gH}$ for $\tilde{\Omega} = 0$.

potential $V_H(H, \phi)$ negatively along the ϕ direction. The location and depth of its minimum remain unchanged, but the corresponding ϕ value shifts from 2π to $2\pi - \tilde{\Omega}$.

Fig. 3 shows the evolution of the chromomagnetic-suppressing potential in terms of ϕ with increasing $\tilde{\Omega}$ at $H \rightarrow 0$ and $r = 0$. It is evident that the potential energy at the physical minimum rises rapidly with increasing $\tilde{\Omega}$. This implies that although the minimum of V_{nonH} still corresponds to $H \rightarrow 0$, its ability to suppress chromomagnetism weakens significantly. Compared to the translational effect of $\tilde{\Omega}$ on V_H , V_{nonH} gradually loses its competitive advantage. Eventually, between the minima of these two potential components, a new global minimum for the total potential emerges. It can be anticipated that as the imaginary angular velocity increases to a critical value

$\tilde{\Omega}_c \in (0, \pi/2)$, the physical ground state will discontinuously jump from $(H, \phi) = (0, 2\pi)$ to a point with $H \neq 0$ and $\phi \in (2\pi - \tilde{\Omega}_c, 2\pi)$. Using the symmetry relation in Eq. (36), a symmetric jump from a point with $H \neq 0$ and $\phi \in (\pi, \pi + \tilde{\Omega}_c)$ to the confining phase at $(H, \phi) = (0, \pi)$ occurs at $\tilde{\Omega} = \pi - \tilde{\Omega}_c$. Thus, the perturbative confinement phase is reached via a first-order transition, and two first-order phase transitions are expected during the emergence of the perturbative confinement phase.

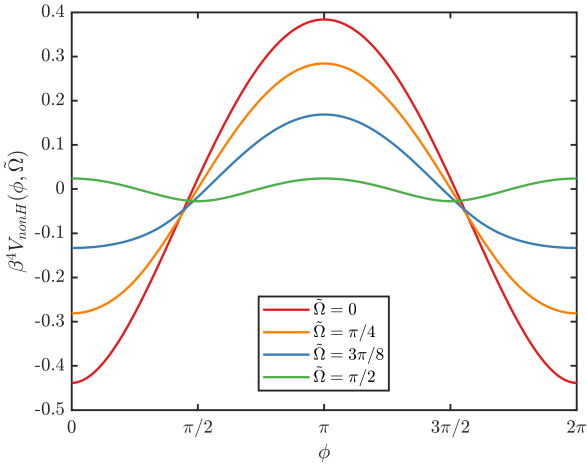


FIG. 3: Evolution of the dimensionless $\beta^4 V_{\text{nonH}}$ chromomagnetic-suppressing potential with ϕ for $\tilde{\Omega} = 0, \pi/4, 3\pi/8, \pi/2$ at $H \rightarrow 0$ and $r = 0$.

IV. PERTURBATIVE CONFINEMENT PHASE TRANSITION AND PHASE DIAGRAM

In the previous section, we made predictions about the nature of the perturbative confinement phase transition based on the effects of V_H and V_{nonH} on chromomagnetism, as well as the reshaped competition between them under rotation. In this section, we perform detailed calculations to explore the phase diagram and properties of the perturbative confinement phase transition.

Fig. 4 shows the evolution of the Polyakov loop potential (with respect to ϕ) with increasing $\tilde{\Omega}$ at $r = 0$ and $T = 10\Lambda$, both in the presence of a chromomagnetic background field (solid lines) and in its absence (dashed lines), along with the corresponding $\beta\sqrt{gH}$. First, we can clearly see that the potential curve with a chromomagnetic background is always lower than that without. In the left panel, the regions where the two curves nearly coincide correspond to very low values of $\beta\sqrt{gH}$ in the right panel, which fluctuate at very low magnitudes and can be considered as vanishing. In regions where the potential curves deviate significantly, the chromomagnetic condensate is induced, and the potential reaches a lower value. The red curve in Fig. 4 for $\tilde{\Omega} = 0$ reproduces the spontaneously broken center symmetry with minima located at $\phi = 0$ and 2π . The orange curve for $\tilde{\Omega} = \pi/2$ has its minimum shifted to $\beta\sqrt{gH} = 0.8$ and $\phi = 3\pi/2$, indicating that the imaginary angular velocity induces a chromomagnetic condensate and further leads to explicit breaking of the center symmetry. The blue curve for $\tilde{\Omega} = \pi$ shows that as $\tilde{\Omega}$ increases, the potential minima deviate from the deconfined vacua to the confined vacuum at $\phi = \pi$.

We can visualize this phase transition by plotting the expectation value of the fundamental Polyakov loop $|L|$ and the scaled chromomagnetic condensate $\beta\sqrt{gH}$ as

functions of $\tilde{\Omega}$ at different temperatures, as shown in Fig. 5. In the left panel, we can see that at different temperatures, $|L|$ undergoes several nontrivial changes during the emergence of the perturbative confinement phase. We need to analyze this step by step. First, the most obvious nontrivial change occurs at imaginary angular velocities symmetric about $\tilde{\Omega} = \pi/2$, where two first-order phase transitions take place, corresponding to jumps in the chromomagnetic field H and the Polyakov loop. This is entirely consistent with our predictions in the previous section. Moreover, due to the suppressing effect of temperature on V_H , the scaled chromomagnetic condensate $\beta\sqrt{gH}$ induced by $\tilde{\Omega}$ becomes smaller at higher temperatures. For $\tilde{\Omega} \in (0, \pi/2)$, a larger $\tilde{\Omega}$ is required to achieve greater suppression of V_{nonH} in order to induce the chromomagnetic condensate. Correspondingly, the critical $\tilde{\Omega}_c \in (\pi/2, \pi)$ for the perturbative confinement transition decreases with increasing temperature, gradually approaching the critical value $\tilde{\Omega}_c = \pi/\sqrt{3}$ for the case without a chromomagnetic background field, indicated by the dashed line in the figure. Second, after the first-order phase transition in the interval $\tilde{\Omega} \in (0, \pi/2)$, the global minimum of the total potential lies between the minima of V_H and V_{nonH} at $(H, \phi) = (0, 2\pi)$ and $(H \neq 0, 2\pi - \tilde{\Omega})$. However, we know that when $\tilde{\Omega}$ becomes even larger, the minimum of V_H rapidly shifts from $\phi = 2\pi$ to $\phi = \pi$. Influenced by this effect, the evolution of ϕ with $\tilde{\Omega}$ also exhibits a turning, descending more rapidly with increasing $\tilde{\Omega}$, and the evolution of the chromomagnetic condensate is also affected to some extent.

Based on the above observations, it is tempting to envision a new phase diagram for the perturbative confinement phase transition on the $T\text{-}\tilde{\Omega}$ plane, as shown in Fig. 6. To better illustrate the temperature dependence of the phase boundary and its asymptotic behavior at high temperatures, we take the horizontal coordinate as $\log_{10} \Lambda^{-1} T$ and the vertical coordinate as $\tilde{\Omega}$. By analyzing the curve for the first-order phase transition boundary, we can see that as temperature increases, the critical $\tilde{\Omega}_c$ decreases and asymptotically approaches the result without chromomagnetism, $\tilde{\Omega}_c = \pi/\sqrt{3}$. Moreover, within the $T\text{-}\tilde{\Omega}$ region where the phase boundary curve is calculated, the critical temperature T_c decreases with increasing $\tilde{\Omega}$. Furthermore, for a fixed $\tilde{\Omega}$, looking from either side of any point on the phase boundary, increasing temperature causes the system to transition from the deconfined phase to the perturbatively confined phase. This contradicts the conventional view that increasing temperature tends to drive the system towards deconfinement. To isolate the pure temperature effect, we have marked three constant- $\tilde{\Omega}$ lines in the figure (from left to right, $\tilde{\Omega}$ increases). The red arrows indicate the direction of increasing temperature, while the blue arrows indicate decreasing temperature. It can be seen that at fixed $\tilde{\Omega}$, the temperature effect still tends to drive the system towards deconfinement, maintaining the conventional picture. Moreover, T_c increases monotonically with $\tilde{\Omega}$.

It is worth noting that the upper limit of temperature

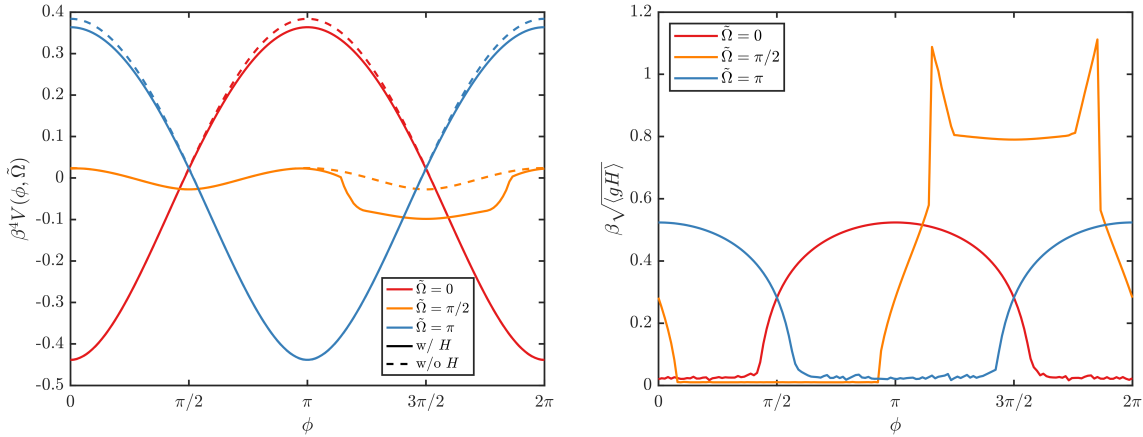


FIG. 4: Evolution of the dimensionless Polyakov loop potential $\beta^4 V$ (left) and the corresponding scaled variable $\beta\sqrt{\langle gH \rangle}$ (right) with ϕ for several values of $\tilde{\Omega}$ at $T = 10\Lambda$ and $r = 0$.

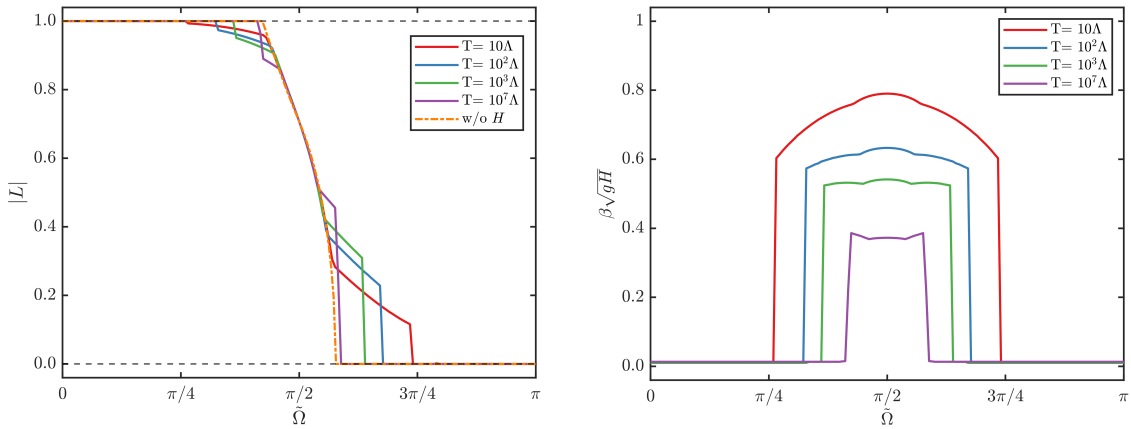


FIG. 5: The expectation value of the fundamental Polyakov loop $|L|$ (left) and the scaled chromomagnetic condensate $\beta\sqrt{gH}$ (right) as functions of $\tilde{\Omega}$ at different temperatures.

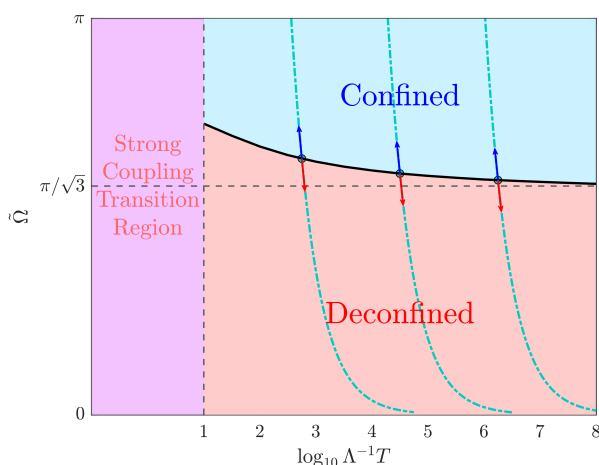


FIG. 6: Phase diagram for the perturbative confinement transition in the T - $\tilde{\Omega}$ plane.

in our calculations here is $T = 10^8\Lambda$. Although asymptotic freedom suggests that higher temperatures are more favorable for perturbative calculations, extremely high temperatures may lose practical physical meaning due to the involvement of other higher-energy physical processes.

The speculated phase diagram on the entire $\tilde{\Omega}$ - T plane in reference [54] has attracted widespread attention and discussion. Through the above research, we find that the introduction of a chromomagnetic background leads to a richer phase structure for the perturbative confinement transition. For comparison, we also plot the phase diagram in Fig. 7 to illustrate our main conclusions. The most obvious change after introducing the chromomagnetic background is that we have identified and confirmed that a larger region at high temperatures belongs to the deconfined region (purple area in the figure). Additionally, the phase boundary curve (blue line) in this region exhibits significant temperature dependence, which dif-

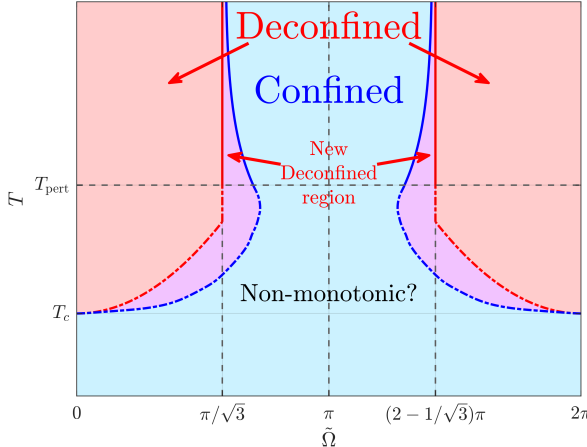


FIG. 7: Conjectured global phase diagram on the $\tilde{\Omega}$ - T plane near the rotation axis ($r = 0$) for SU(2) Yang-Mills theory, with curves representing phase transitions.

fers from previous conclusions (red line). Regarding the order of the phase transition, considering the excitation effect of $\tilde{\Omega}$ on the chromomagnetic condensate and the explicit breaking of $\mathbb{Z}(2)$ symmetry, our results suggest that the perturbative confinement transition is first-order rather than second-order. In the low-temperature non-perturbative region, as analyzed in references [54, 67], the Kugo-Ojima-Gribov-Zwanziger (KOGZ) mechanism [68–70] causes the ghost fields, which cancel unphysical polarization modes at high temperatures, to make the system increasingly confining uniformly for any $\tilde{\Omega}$. However, our perturbative calculations indicate that before entering the non-perturbative temperature region, there might still be an interval where the critical $\tilde{\Omega}_c$ increases with decreasing temperature. From an overall perspective, however, there should exist a general trend in the non-perturbative regime where the critical value $\tilde{\Omega}_c$ increases with rising temperature. From the standpoint of phase boundary continuity, it is entirely possible that the phase boundary exhibits non-monotonic behavior within the non-perturbative regime, indicating the presence of complex non-perturbative effects. This would, of course, significantly impact the adiabatic continuity evolution path without a phase transition—connecting the perturbatively confined phase and the conventional confined phase—as mentioned in reference [54]. Last but not least, given that the non-perturbative deconfinement transition in SU(2) theory is of second order [66], a critical end point (CEP) may exist, connecting the first-order perturbative confinement transition and the second-order non-perturbative deconfinement transition.

V. ANALYTICAL CONTINUATION TO REAL ROTATION.

As mentioned earlier, due to the sign problem in lattice calculations, in order to obtain results for real angular velocity corresponding to physical reality, the lattice method extrapolates the dependence of related physical quantities (such as T_c on Ω) via the relation $\Omega^2 = -\omega^2$. To be precise, they must obtain the dependence on Ω^2 to perform a smooth analytic continuation. For instance, the Tolman-Ehrenfest effect verified in reference [71] also depends on Ω^2 .

In reference [54], it was found that the local effective potential fully satisfies the dependence on Ω^2 . However, as stated in that work, their study of imaginary angular velocity is based on the series expansion $\ln(1 - z) = -\sum_{n=1}^{\infty} z^n/n$ for $|z| \leq 1$. Performing the continuation $\Omega^2 = -\omega^2$ directly on this basis effectively uses the series expansion in the region $|z| > 1$, which is entirely incorrect. However, direct calculation presents other problems, as introducing a real angular velocity is equivalent to introducing an effective chemical potential. For a bosonic system, the chemical potential must satisfy $|\mu| \leq m$. Since the W^\pm gauge bosons in our calculation are massless, this leads to an infrared singularity. This singularity originates from a violation of causality because, from the conventional view $k_n = 2\pi n/L$, low-momentum modes imply the system's boundary is at infinity, which contradicts the finiteness of a rotating system. There are two approaches to address this singularity [41]. One is to still consider transverse momentum k_\perp as continuously varying and deem modes with $k_\perp < \omega$ as unphysical, applying an infrared cutoff to this part. The other is to impose boundary conditions so that the system's lowest transverse momentum k_\perp^{\min} self-consistently exceeds ω .

Since it is difficult to establish a direct relationship between low-momentum modes and superluminal behavior (i.e., determining at which momentum the mode becomes acausal) and one can only simplistically assume that the singular transverse momentum states with $k_\perp < \omega$ are superluminal, while still treating transverse momentum k_\perp as continuous (which inherently assumes an infinite boundary), this cutoff method in our calculation would directly lose the crucial contribution from the LLL, which is clearly unphysical. Therefore, we adopt the second approach by imposing the following boundary condition:

$$F(-\lambda_k^l, |l| + 1, X) = 0, \quad X = \frac{1}{2}gHR^2 \quad (37)$$

to obtain the finite-temperature part of the potential at $r = 0$ (details in Appendix B):

$$V_T(\vec{0}) = \frac{T}{(2\pi)^2} \sum_{s=\pm} \sum_k \frac{gH}{N_k^0} \int_{-\infty}^{+\infty} \frac{dk_z}{2\pi} \ln \left(1 - e^{-\beta(\omega_s^0 + s\omega) + i\phi} \right) + \ln \left(1 - e^{-\beta(\omega_s^0 - s\omega) - i\phi} \right). \quad (38)$$

Here,

$$N_k^0 = \frac{1}{2\pi} \int_0^X dx F(-\lambda_k^0, 1, x)^2 e^{-x}, \quad (39)$$

$$\omega_s^0 = \sqrt{k_z^2 + (2\lambda_k^0 + 2s + 1)gH}. \quad (40)$$

In subsequent calculations, we set $TR = 1.5$ to be consistent with the parameters used in reference [54]. It can be verified that in the limit $H \rightarrow 0$, the result reduces to that in [54] (see Appendix C). Now we need to discuss whether imposing boundary conditions self-consistently resolves the infrared divergence issue. Firstly, for the Savvidy model, its LLL inherently possesses a long-wavelength instability in the quadratic approximation, so theoretically, imposing boundary conditions cannot resolve the intrinsic instability of the Savvidy model itself. We need to verify whether, for higher Landau levels, the transverse momenta k_\perp for the first excited state with $s = -1$ and the ground state with $s = 1$, which are $\sqrt{(2\lambda_2^0 - 1)gH}$ and $\sqrt{(2\lambda_1^0 + 1)gH}$ respectively, are greater than $\omega_{\max} = 1/R$. As shown in Fig. 8, within the range of $\beta\sqrt{gH}$ values achievable in subsequent calculations, the boundary condition indeed resolves this problem.

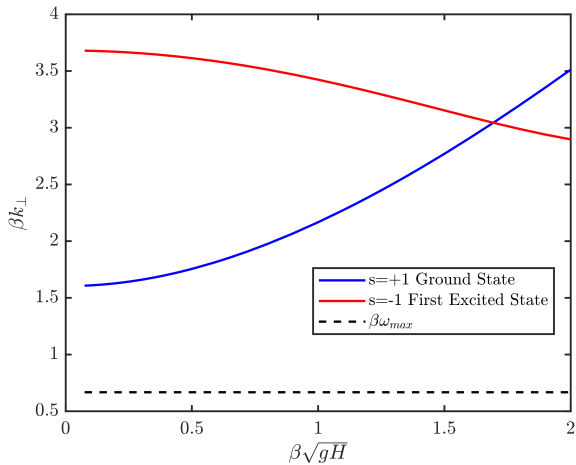


FIG. 8: The normalized transverse momenta βk_\perp for the first excited state ($s = -1$) and the ground state ($s = 1$) as functions of $\beta\sqrt{gH}$, compared with $\beta\omega_{\max}$.

However, two issues remain in our system. First, regarding the long-wavelength instability of the LLL, we follow the convention of previous literature and take the real part of this contribution. Second, there is the singularity arising from the complex chemical potential. When both the real angular velocity and the Polyakov loop are non-zero, the modification to the Matsubara frequencies becomes a complex number with non-zero real and imaginary parts: $-\beta s\omega + i\phi$, equivalent to introducing a complex chemical potential. Consequently, the contributions from the two polarization modes $s = \pm$ to the potential are not real. In the absence of a chromomagnetic background, since the single-particle spectrum $|\vec{k}|$ has no spin

dependence, these contributions cancel overall. However, due to the coupling between the chromomagnetic field and spin, ω_s^0 now differs with spin, leading to an imaginary part in the overall potential. Here, we still study the real part of the potential. Nevertheless, subsequent calculations of the Polyakov loop potential reveal that for any angular velocity, Although a singularity emerges in the local vicinity, the physical minimum itself remains well-defined and is located at $\phi = 0$ and 2π .

We have performed the numerical integration and summation of Eq. (38) for real ω . The sums over k and the k_z integration are cut off at sufficiently large numbers, and convergence is confirmed. It should be noted that numerically achieving $H = 0$ remains unfeasible. We set a lower limit of $\beta\sqrt{gH} = 0.075$, and the numerical results for the potential at this value show convergence to the result without chromomagnetism.

Fig. 9 shows the evolution of the Polyakov loop potential (solid lines with chromomagnetic field, dashed lines without) with increasing ω at $r = 0$ and $T = 10\Lambda$, along with the corresponding scaled variable $\beta\sqrt{gH}$. The potential curve with a chromomagnetic background remains lower than that without. In regions where the two curves nearly coincide, $\beta\sqrt{gH}$ is near our set lower limit and can be considered as vanished. The potential minima are located at $\phi = 0 \bmod 2\pi$ for any ω , indicating the system remains in the deconfined phase. However, a point of caution: when $\omega \neq 0$, the minimum of our Polyakov loop potential is a cusp (unlike the case with imaginary angular velocity), where the first derivative does not exist. This implies the potential curvature around the minimum, which defines the Debye screening mass, lacks a traditional definition. The reason is that the local thermodynamic potential at the minimum possesses an imaginary part due to the complex chemical potential. In contrast, for $\omega = 0$, the effective chemical potential is always imaginary, avoiding the singularity from a real effective chemical potential. Although long-wavelength instability ($k_\perp^{\text{LLL}} < 0$) persists in the LLL near $\phi = 0$, the minimum is a stable point with zero first derivative. Based on the preceding discussion, the emergence of a cusp in the Polyakov loop potential under real rotation manifests in a fundamental alteration of local stability and suggests a novel singularity within the phase structure. This behavior indicates that the system's properties near the minimum may not be fully captured by conventional equilibrium thermodynamics, as the effective complex chemical potential arising from the coupling between rotation, spin, and the chromomagnetic field introduces an imaginary component of Polyakov loop potential.

Fig. 10 shows the variation of the chromomagnetic condensate with real angular velocity (black solid line). In contrast to the previous case with imaginary angular velocity, for $T = 10\Lambda$, the chromomagnetic condensate exists across the entire ω range. This is a consequence of the boundary conditions, which change the Landau level quantum numbers from uniformly spaced $m \in \mathbb{N}$ to non-uniformly spaced λ_k , increasing the energy gaps and

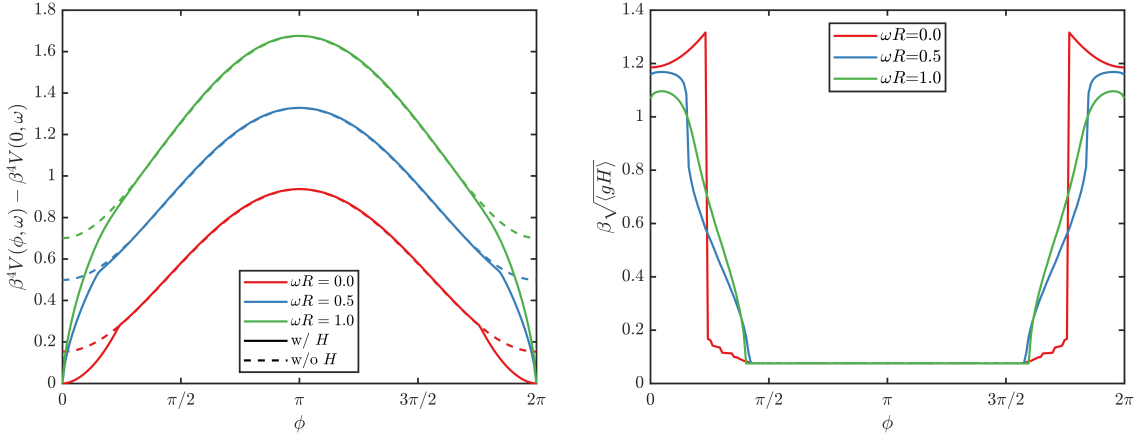


FIG. 9: Evolution of the dimensionless Polyakov loop potential $\beta^4 V$ (left) and the corresponding scaled variable $\beta\sqrt{\langle gH \rangle}$ (right) with ϕ for several values of the real angular velocity ω at $T = 10\Lambda$ and $r = 0$.

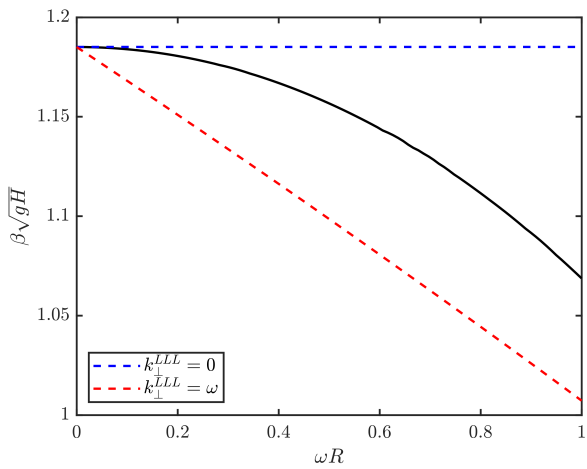


FIG. 10: Evolution of the scaled chromomagnetic condensate $\beta\sqrt{gH}$ as a function of the real angular velocity ω , with dashed lines indicating $k_\perp^{\text{LLL}} = 0$ and $k_\perp^{\text{LLL}} = \omega$.

significantly suppressing contributions from higher Landau levels. Consequently, the system is dominated by the LLL. As the angular velocity increases, the chromomagnetic condensate becomes smaller. In previous studies [72], the coupling of the chromomagnetic field to the quark system alters the chiral condensate and the chiral phase transition temperature, suggesting a possibility that rotation-induced changes in the chromomagnetic field could indirectly affect the chiral phase transition. The blue dashed line represents the chromomagnetic condensate value when $k_\perp^{\text{LLL}} = 0$, and the red dashed line represents the value when $k_\perp^{\text{LLL}} = \omega$. Our calculated chromomagnetic condensate lies below the black dashed line and above the red dashed line, indicating $k_\perp^{\text{LLL}} \in [0, \omega]$. Under this treatment, the long-wavelength instability per-

sists, but its nature changes from the traditional type caused by $k_\perp^{\text{LLL}} < 0$ leading to an imaginary spectrum, to a type caused by $k_\perp^{\text{LLL}} < \omega$ leading to a negative energy spectrum.

VI. SUMMARY AND OUTLOOK

The reappearance of non-perturbative physics in the perturbative regime driven by an imaginary angular velocity is highly intriguing. As our results demonstrate, the imaginary angular velocity not only induces a perturbative confinement phase but also triggers chromomagnetic condensation, exerting significant and non-trivial influences on the phase diagram of the perturbative confinement transition.

Through analysis, we decompose the effective potential into two components: the chromomagnetic-favoring potential V_H and the chromomagnetic-suppressing potential $V_{\text{non}H}$. We systematically study the effects of temperature and imaginary angular velocity on these components, thereby elucidating the microscopic mechanism by which $\tilde{\Omega}$ induces the chromomagnetic condensate: the imaginary angular velocity shifts the minimum of V_H along the ϕ direction while significantly weakening the suppressing effect of $V_{\text{non}H}$ on chromomagnetism, thereby altering the competitive balance between them. This leads us to obtain a first-order phase boundary with explicit temperature dependence, identified by the discontinuous jump of the order parameters $|L|$ and H at the critical point. This phase boundary asymptotically approaches the theoretical value for the case without a chromomagnetic background, $\tilde{\Omega}_c = \pi/\sqrt{3}$, at high temperatures.

We thereby construct a new phase diagram, identifying and confirming that within the $\tilde{\Omega}$ - T phase structure, a more extensive region at high temperatures belongs to the deconfined phase. The perturbative con-

finement transition consequently exhibits a richer phase structure, which directly manifests the complex coupling between the chromomagnetic field and the Polyakov loop. Under the reasonable assumption of a continuous phase boundary, by analyzing its trend before entering the non-perturbative temperature regime, we speculate that non-monotonic behavior of the phase boundary may occur in the non-perturbative regime, revealing the possible complex non-perturbative effects therein. This could significantly impact the adiabatic continuity evolution path connecting the perturbatively confined phase and the conventional confined phase. Given the second-order nature of the non-perturbative deconfinement transition in $SU(2)$ theory, a critical end point (CEP) may exist where it meets the first-order perturbative confinement transition.

Finally, we investigate the effects of a real angular velocity ω . Adopting the conventional treatment, we impose boundary conditions to preserve causality and take the real part for the Savvidy instability (LLL) in the quadratic approximation. Our study finds that the effective complex chemical potential introduced by the real angular velocity, due to the coupling between the chromomagnetic field and spin, prevents the imaginary contributions from the two spin polarization states ($s = \pm$) from canceling each other, resulting in a non-zero imaginary part in the total potential. This leads to a **cusp** (discontinuous first derivative) at the minimum of the Polyakov loop potential, implying the traditional Debye screening mass cannot be defined at this point. This phenomenon reflects the possible complex non-equilibrium evolution when the chromomagnetic field, rotation, and spin are coupled. Furthermore, we observe that the strength of the chromomagnetic condensate decreases with increasing real angular velocity. Throughout this process, the long-wavelength instability of the LLL in the quadratic approximation persists, but its character changes: the instability threshold shifts from the traditional condition $k_{\perp}^{\text{LLL}} < 0$ (leading to an imaginary spectrum) to $k_{\perp}^{\text{LLL}} < \omega$ (leading to a negative energy spectrum).

Imaginary angular velocity can open a new pathway to study non-perturbative physics within a perturbative framework. A natural extension is to introduce dynamical quarks to explore whether imaginary rotation can also induce chiral symmetry breaking in the perturbative regime. If realized, it would suggest that key non-perturbative features—including confinement, chiral symmetry breaking, and chromomagnetic condensation—could be systematically accessed via perturbative methods under imaginary rotation. Furthermore, generalizing the analysis to $SU(3)$ gauge theory would provide a more direct link to QCD. Finally, the predictions from our $\tilde{\Omega}$ - T phase diagram, particularly the induced chromomagnetic condensate and the first-order transition boundary, offer concrete targets for future lattice simulations, which are crucial for mapping the complete phase structure of rotating gauge theories.

ACKNOWLEDGMENTS

We acknowledge helpful discussions with Hao-Lei Chen, Defu Hou and Xuguang Huang. This work is supported in part by the National Natural Science Foundation of China (NSFC) Grant Nos: 12235016, 12221005, 12147150, 12505148. Recently, we learned that Ref. [73] addresses a similar topic, which was posted on arXiv on the same day.

Appendix A: THE ROTATION-MODIFIED LAGRANGIAN DENSITY

Since the derivative operator appears in the Lagrangian only in the form $\partial_{[\mu}\square_{\nu]}$, the transformation of the entire system satisfies the identity (8). After changing the ordinary derivatives in $B_{\mu\nu}$ to covariant derivatives and introducing the Polyakov background field, we have:

$$B_{\mu\nu} \rightarrow \partial_{[\mu} B_{\nu]} + \delta_{[\mu 0} R_0 B_{\nu]}. \quad (\text{A1})$$

Since

$$\begin{aligned} R_0 B_k &= -\omega \epsilon_{j3} x_j \partial_i B_k + \omega \epsilon_{k3} B_i \\ &= \frac{1}{2} H (-\omega \epsilon_{j3} x_j \partial_i (\epsilon_{k3} x_j) + \omega \epsilon_{k3} \epsilon_{ij3} x_j) \\ &= \frac{1}{2} H (-\omega \epsilon_{j3} \epsilon_{k3} x_j + \omega \epsilon_{k3} \epsilon_{ij3} x_j) = 0, \end{aligned} \quad (\text{A2})$$

the tensor $B_{\mu\nu}$ remains unchanged, and consequently the term $B_{\mu\nu} B^{\mu\nu}$ that gives rise to H^2 is also unchanged. Ultimately, the effect of rotation originates primarily from the kinetic term $\hat{Q}_{\mu\nu}^+ \hat{Q}_{\mu\nu}^-$. With

$$D_\mu \rightarrow D_\mu + \delta_{\mu 0} (ig B_0 + R_0), \quad (\text{A3})$$

we compute the additional part \mathcal{L}_{add} of the Lagrangian to reduce the computational burden, i.e., $\mathcal{L}_0 \rightarrow \mathcal{L}_0 + \mathcal{L}_{\text{add}}$, where

$$\hat{Q}_{\mu\nu}^+ \rightarrow \hat{Q}_{\mu\nu}^+ + \delta_{0[\mu} (ig B_0 + R_0) Q_{\nu]}^+, \quad (\text{A4})$$

$$\hat{Q}_{\mu\nu}^- \rightarrow \hat{Q}_{\mu\nu}^- + \delta_{0[\mu} (-ig B_0 + R_0) Q_{\nu]}^-. \quad (\text{A5})$$

Thus, we obtain

$$-\frac{1}{2} \hat{Q}_{\mu\nu}^+ \hat{Q}_{\mu\nu}^- \rightarrow -\frac{1}{2} \hat{Q}_{\mu\nu}^+ \hat{Q}_{\mu\nu}^- + \mathcal{L}_{\text{add}}, \quad (\text{A6})$$

with

$$\begin{aligned} \mathcal{L}_{\text{add}} &= - \left[\hat{Q}_{0i}^+ (-ig B_0 + R_0) Q_{i-}^+ + \hat{Q}_{i-}^+ (ig B_0 + R_0) Q_i^+ \right. \\ &\quad \left. + (ig B_0 + R_0) Q_i^+ \delta_0^{[0} (-ig B_0 + R_0) Q_{i-}^{\nu]} \right]. \end{aligned} \quad (\text{A7})$$

Using

$$\begin{aligned} &(ig B_0 + R_0) Q_{\nu}^+ \delta_0^{[0} (-ig B_0 + R_0) Q_{i-}^{\nu]} \\ &= g^2 B_0^2 Q_i^+ Q_{i-}^+ + (R_0 Q_i^+) (R_0 Q_{i-}^+) \\ &\quad + ig B_0 (Q_i^+ R_0 Q_{i-}^+ - Q_i^- R_0 Q_i^+), \end{aligned} \quad (\text{A8})$$

and noting the symmetry $\mathcal{L}_{\text{add}} = \mathcal{L}_{\text{add}}^\dagger$, the equations of motion (EOM) for Q^+ and Q^- are conjugate to each

other. By solving the Euler-Lagrange equation

$$\left[\frac{\partial}{\partial Q_\nu^-} - \partial_\mu \frac{\partial}{\partial (\partial_\mu Q_\nu^-)} \right] \mathcal{L}_{\text{add}}, \quad (\text{A9})$$

we obtain the additional terms that need to be added to the EOM without rotation.

For the temporal component $\nu = 0$:

$$\partial_i (igB_0 + R_0) Q_i^+ + igB_i (igB_0 + R_0) Q_i^+ = igB_0 (D_i Q_i^+) + \partial_i (R_0 Q_i^+) + igB_i R_0 Q_i^+ = (igB_0 - \omega i \hat{L}_z) (D_i Q_i^+). \quad (\text{A10})$$

For the spatial components $\nu = i$:

$$\begin{aligned} & (g^2 B_0^2 - igB_0 R_0) Q_i^+ + \omega \epsilon_{ik3} (igB_0 + R_0) Q_k^+ - (igB_0 Q_{0i}^+ - \omega Q_{0k}^+ \epsilon_{ik3}) - \partial_0 (igB_0 + R_0) Q_i^+ + i\omega \hat{L}_z Q_{0i}^+ \\ & + i\omega \hat{L}_z (igB_0 + R_0) Q_i^+ + (igB_i igB_0 + \omega \epsilon_{0\nu i3} igB_\nu - ig\omega \epsilon_{0\rho\mu 3} x_\rho \partial_\mu B_\nu - ig\omega B_i \epsilon_{0\rho\mu 3} x_\rho \partial_\mu) Q_0^+ \\ & = [g^2 B_0^2 - 2igB_0 (\partial_0 - i\omega \hat{L}_z) + \omega^2 (1 - \delta_{i3}) + 2i\omega \hat{L}_z \partial_0 + \omega^2 \hat{L}_z^2] Q_i^+ \\ & + [2\omega igB_0 + 2(\partial_0 - i\omega \hat{L}_z) \omega] \epsilon_{ik3} Q_k^+ + D_i (igB_0 - \omega i \hat{L}_z) Q_0^+. \end{aligned} \quad (\text{A11})$$

It can be seen that the inclusion of angular velocity significantly affects the equations of motion, particularly through a strong coupling with Q_0 . If, under a suitable gauge condition, the coupling between Q_0 and the spatial components can be eliminated, it would greatly simplify our study of the spin gluons Q_\pm . Substituting the additional terms into the original EOM and analyzing the temporal component $\nu = 0$:

$$\begin{aligned} & (\partial_0^2 - D_i^2) Q_0^+ - \partial_0 (\partial_0 Q_0^+ - D_i Q_i^+) + (igB_0 - \omega i \hat{L}_z) (D_i Q_i^+) \\ & = (\partial_0^2 - D_i^2) Q_0^+ - \partial_0^2 Q_0^+ + (\partial_0 + igB_0 - \omega i \hat{L}_z) D_i Q_i^+ \\ & = [(\partial_0 + igB_0 - \omega i \hat{L}_z)^2 - D_i^2] Q_0^+ - (\partial_0 + igB_0 - \omega i \hat{L}_z)^2 Q_0^+ + (\partial_0 + igB_0 - \omega i \hat{L}_z) D_i Q_i^+ \\ & = D_\mu D^\mu Q_0^+ - D_0 (D_\mu Q^{+, \mu}) = 0. \end{aligned} \quad (\text{A12})$$

By replacing the covariant derivative as $\partial_0 \rightarrow D_0 = \partial_0 + igB_0 - \omega i \hat{L}_z$ and choosing the gauge condition:

$$D_\mu Q^{+, \mu} = 0, \quad (\text{A13})$$

we can eliminate the coupling between Q_0 and Q_i in the temporal component of the equation. Analyzing the part involving Q_0^+ in the spatial components:

$$-D^i (\partial_0 Q_0^+ - D_i Q_i^+) + D_i (igB_0 - \omega i \hat{L}_z) Q_0^+ = D_i (D_\mu Q^{+, \mu}) = 0. \quad (\text{A14})$$

Thus, we have successfully decoupled the temporal and spatial components in the equations of motion. In this new gauge, the additional terms in the equations of motion become:

$$\nu = 1 : [g^2 B_0^2 - 2igB_0 (\partial_0 - i\omega \hat{L}_z) + 2i\omega \hat{L}_z \partial_0 + \omega^2 \hat{L}_z^2 + \omega^2] Q_1^+ - 2i\omega (i\partial_0 - gB_0 + \omega \hat{L}_z) Q_2^+, \quad (\text{A15})$$

$$\nu = 2 : [g^2 B_0^2 - 2igB_0 (\partial_0 - i\omega \hat{L}_z) + 2i\omega \hat{L}_z \partial_0 + \omega^2 \hat{L}_z^2 + \omega^2] Q_2^+ + 2i\omega (i\partial_0 - gB_0 + \omega \hat{L}_z) Q_1^+, \quad (\text{A16})$$

$$\nu = 3 : [g^2 B_0^2 - 2igB_0 (\partial_0 - i\omega \hat{L}_z) + 2i\omega \hat{L}_z \partial_0 + \omega^2 \hat{L}_z^2] Q_3^+. \quad (\text{A17})$$

Transforming the additional terms in the EOM to the spin components $Q_\pm^+ = Q_1^+ \pm iQ_2^+$, the equations take the form:

$$\begin{pmatrix} \hat{L}_1 & \hat{L}_2 \\ -\hat{L}_2 & \hat{L}_1 \end{pmatrix} \begin{pmatrix} Q_1^+ \\ Q_2^+ \end{pmatrix} = X^{-1} \begin{pmatrix} \hat{L}_1 & \hat{L}_2 \\ -\hat{L}_2 & \hat{L}_1 \end{pmatrix} X X^{-1} \begin{pmatrix} Q_1^+ \\ Q_2^+ \end{pmatrix} = \text{diag}(\hat{L}_1 - i\hat{L}_2, \hat{L}_1 + i\hat{L}_2) \begin{pmatrix} Q_1^+ \\ Q_2^+ \end{pmatrix} = 0, \quad (\text{A18})$$

where

$$X = \begin{pmatrix} 1 & 1 \\ -i & i \end{pmatrix}, \quad X^{-1} = \frac{1}{2} \begin{pmatrix} 1 & i \\ 1 & -i \end{pmatrix}, \quad (\text{A19})$$

$$\hat{L}_1 = g^2 B_0^2 - 2igB_0 (\partial_0 - i\omega \hat{L}_z) + 2i\omega \hat{L}_z \partial_0 + \omega^2 \hat{L}_z^2 + \omega^2, \quad (\text{A20})$$

$$\hat{L}_2 = -2i\omega (i\partial_0 - gB_0 + \omega \hat{L}_z). \quad (\text{A21})$$

These additional terms will shift the time derivative ∂_0 in the original equation. For $\hat{L}_1 - si\hat{L}_2$ with $s = \pm 1$, we have:

$$\begin{aligned}
(i\partial_0)^2 + \hat{L}_1 - is\hat{L}_2 &= g^2 B_0^2 - 2igB_0(\partial_0 - i\omega\hat{L}_z) + 2i\omega\hat{L}_z\partial_0 + \omega^2\hat{L}_z^2 + \omega^2 + (i\partial_0)^2 - 2\omega s(i\partial_0 - gB_0 + \omega\hat{L}_z) \\
&= (i\partial_0 + \omega\hat{L}_z)^2 - 2gB_0(i\partial_0 + \omega\hat{L}_z) + g^2 B_0^2 + \omega^2 - 2\omega s(i\partial_0 - gB_0 + \omega\hat{L}_z) \\
&= (i\partial_0 - gB_0 + \omega\hat{L}_z)^2 + \omega^2 - 2\omega s(i\partial_0 - gB_0 + \omega\hat{L}_z) \\
&= [i\partial_0 - gB_0 + \omega(\hat{L}_z - s)]^2.
\end{aligned} \tag{A22}$$

Thus, the angular velocity shifts the energy levels according to Eq. (10). The eigenmodes remain unchanged, and the coupling forms between the Landau level quantum number and spin, and between the angular momentum quantum number and spin, are $m + s$ and $l - s$, respectively. Substituting into the gauge condition, this exactly corresponds to the recurrence relation between L_m^l and L_{m+s}^{l-s} , indicating that the chosen orientation of the magnetic field is appropriate.

In the imaginary-time formalism of finite temperature field theory, the zero component of all covariant vectors, such as the time component of four-dimensional space-time, is transformed with $\tau = -it$. Similarly, the zero component of the electromagnetic four-vector potential becomes $B_0 \rightarrow -iB_0 = -i(g\beta)^{-1}\phi$. Taking the imaginary angular velocity $\omega = i\Omega$, we obtain:

$$\partial_0 \rightarrow i\partial_\tau + \phi/\beta + \Omega(\hat{L}_z - s). \tag{A23}$$

Appendix B: CAUSALITY BOUND IN THE ROTATING FRAME

The inclusion of boundary conditions deforms the Landau wave functions due to finite-size effects:

$$\tilde{\Phi}_\lambda^{(l)}(\rho, \phi) = \frac{1}{|l|!} \sqrt{\frac{gH}{2\pi}} \sqrt{\frac{\Gamma(\lambda + |l| + 1)}{\Gamma(\lambda + 1)}} F(-\lambda, |l| + 1, X) \cdot X^{|l|/2} e^{-\frac{1}{2}X} e^{il\phi}. \tag{B1}$$

Here, $F(-\lambda, |l| + 1, x)$ represents the confluent hypergeometric function, also known as Kummer's function of the first kind. It satisfies the boundary condition:

$$F(-\lambda, |l| + 1, X) = 0, \quad X = \frac{1}{2}gHR^2. \tag{B2}$$

The quantum number λ is thereby discretized into $\lambda_k^{|l|}$, denoting the k -th root of $F(-\lambda, |l| + 1, X) = 0$. The orthogonality condition is given by:

$$\int_0^X dx F(-\lambda_k^{|l|}, |l| + 1, x) F(-\lambda_{k'}^{|l|}, |l| + 1, x) x^{|l|} e^{-x} = N \delta_{kk'}. \tag{B3}$$

We define the normalization constant for the radial part as:

$$N_k^{|l|} = \frac{1}{2\pi} \int_0^{2\pi} d\phi \int_0^R \rho d\rho |\tilde{\Phi}_{\lambda_k^{|l|}}^{(l)}(\rho, \phi)|^2 = \frac{1}{2\pi} \frac{1}{|l|!^2} \frac{\Gamma(\lambda + |l| + 1)}{\Gamma(\lambda + 1)} \int_0^X dx F(-\lambda_k^{|l|}, |l| + 1, x)^2 x^{|l|} e^{-x}. \tag{B4}$$

To compute the spectral density $\sum_\lambda \langle \lambda | \lambda \rangle$, we note that the quantum state of the system is described by $|\lambda\rangle = |\lambda_k^{|l|}, l, k_z\rangle$. We have:

$$\langle \lambda_{k'}^{|l'|}, l', k_z' | \lambda_k^{|l|}, l, k_z \rangle = \int d^3\vec{x} \langle \lambda_k^{|l|}, l, k_z | \vec{x} \rangle \langle \vec{x} | \lambda_k^{|l|}, l, k_z \rangle = 2\pi \delta_{l,l'} \cdot 2\pi \delta(k_z - k_z') \cdot N_k^{|l|}. \tag{B5}$$

Using $\sum_\lambda \langle \lambda' | \lambda \rangle = 1$, we obtain the spectral density:

$$\sum_\lambda = \frac{1}{2\pi} \sum_l \sum_k (N_k^{|l|})^{-1} \int_{-\infty}^{+\infty} \frac{dk_z}{2\pi}. \tag{B6}$$

The finite-temperature potential is given by:

$$\begin{aligned} V_T &= \sum_{s=\pm} \frac{T}{2\pi} \sum_l \sum_k \frac{|\tilde{\Phi}_{\lambda_k^{|l|}}^{(l)}(\rho, \phi)|^2}{N_k^{|l|}} \int_{-\infty}^{+\infty} \frac{dk_z}{2\pi} \ln \left(1 - e^{-\beta \omega_s + i[\phi + (l-s)\tilde{\Omega}]} \right) + \ln \left(1 - e^{-\beta \omega_s - i[\phi + (l-s)\tilde{\Omega}]} \right)_{\Omega=-i\omega} \\ &= \sum_{s=\pm} \frac{T}{2\pi} \sum_l \sum_k \frac{|\tilde{\Phi}_{\lambda_k^{|l|}}^{(l)}(\rho, \phi)|^2}{N_k^{|l|}} \int_{-\infty}^{+\infty} \frac{dk_z}{2\pi} \ln \left(1 - e^{-\beta [\omega_s - (l-s)\omega] + i\phi} \right) + \ln \left(1 - e^{-\beta [\omega_s + (l-s)\omega] - i\phi} \right), \end{aligned} \quad (\text{B7})$$

with the corresponding eigen-spectrum:

$$\omega_s = \sqrt{k_z^2 + (2\lambda_k^{|l|} + 2s + |l| - l + 1)gH}. \quad (\text{B8})$$

To study the thermodynamic potential at $\vec{r} = 0$, we utilize the property:

$$\lim_{\vec{r} \rightarrow 0} |\tilde{\Phi}_{\lambda_k^{|l|}}^{(l)}(\rho, \phi)|^2 = \frac{gH}{2\pi} \delta_{l,0}, \quad (\text{B9})$$

from which we can derive the thermodynamic potential in Eq. (38).

Appendix C: THE LIMIT OF VANISHING CHROMOMAGNETIC FIELD

We first examine the limit of vanishing chromomagnetic field, $H \rightarrow 0$, under an imaginary angular velocity.

$$\Delta k_\perp^2 = 2gH : \frac{gH}{2\pi} \sum_{m=0}^{+\infty} = \frac{gH}{2\pi} \sum_{m=0}^{+\infty} \frac{dk_\perp^2}{\Delta k_\perp^2} = \int_0^\infty \frac{dk_\perp^2}{4\pi}. \quad (\text{C1})$$

The summation over Landau levels transforms into an integral. For the tachyonic mode, we have:

$$u(-, 0, \vec{0}) = \lim_{H \rightarrow 0} \frac{gH}{\pi\beta} \int_{-\infty}^{+\infty} \frac{dk}{2\pi} \text{Re} \ln \left(1 - e^{-\beta \sqrt{k^2 - gH} + i(\phi + \tilde{\Omega})} \right) = \lim_{H \rightarrow 0} \frac{2gH}{\pi\beta} \int_0^{\sqrt{gH}} \frac{dk}{2\pi} \text{Re} \ln \left(1 - e^{-\beta \sqrt{k^2 - gH} + i(\phi + \tilde{\Omega})} \right). \quad (\text{C2})$$

Utilizing the mean value theorem,

$$\int_a^b dx f(x) = f(\epsilon)(b-a), \quad \epsilon \in [a, b], \quad (\text{C3})$$

$$\lim_{x \rightarrow 0^+} x^3 \ln(1 - e^{-ix}) = 0, \quad (\text{C4})$$

we find that $u(-, 0, \vec{0}) = 0$. Similarly, $u(-, 1, \vec{0}) = 0$. Consequently, the finite-temperature thermodynamic potential reduces to:

$$\begin{aligned} V_T(\vec{0}) &= T \sum_{s=\pm} \int \frac{dk_\perp^2 dk_z}{8\pi} 2 \text{Re} \ln \left(1 - e^{-\beta |\vec{k}| + i(\phi - s\tilde{\Omega})} \right) \\ &= 2T \int \frac{4\pi k^2 dk}{(2\pi)^3} - \sum_{n=1}^{\infty} \frac{1}{n} e^{-n\beta k} \sum_{s=\pm} \cos n(\phi - s\tilde{\Omega}) \\ &= -\frac{2T^4}{\pi^2} \sum_{s=\pm} \sum_{n=1}^{\infty} \frac{1}{n^4} \cos n(\phi - s\tilde{\Omega}) \\ &= \frac{2\pi^2 T^4}{3} \sum_{s=\pm} B_4 \left[\frac{1}{2\pi} (\phi - s\tilde{\Omega}) \right]_{\text{mod } 1}. \end{aligned} \quad (\text{C5})$$

Next, we examine the limit $H \rightarrow 0$ under a real angular velocity. In the limit $X \rightarrow 0$, we have [74]:

$$e^{-X/2} F(-\lambda, 1, X) \rightarrow J_0(\sqrt{4\lambda X}). \quad (\text{C6})$$

The zeros satisfy:

$$\lambda_k^0 \rightarrow \frac{\epsilon_k^0}{4X}, \quad J_0(\epsilon_k^0) = 0. \quad (\text{C7})$$

The normalization constant becomes:

$$\begin{aligned} N_k^0 &= \frac{1}{2\pi} \int_0^X dx F(-\lambda_k^0, 1, x)^2 e^{-x} \\ &= \frac{1}{2\pi} \int_0^1 X d\hat{r}^2 F(-\lambda_k^0, 1, X\hat{r}^2)^2 e^{-X\hat{r}^2} \\ &\rightarrow \frac{X}{\pi} \int_0^1 \hat{r} d\hat{r} J_0(\epsilon_k^0 \hat{r})^2 = \frac{X}{2\pi} J_1^2(\epsilon_k^0). \end{aligned} \quad (\text{C8})$$

The energy spectrum simplifies to:

$$\omega_s^0 = \sqrt{k_z^2 + (2\lambda_k^0 + 2s + 1)gH} \rightarrow \sqrt{k_z^2 + (\epsilon_k^0/R)^2}, \quad (\text{C9})$$

which no longer depends on spin and is denoted as ω^0 . Substituting into Eq. (38), we obtain the thermodynamic potential in the limit of a vanishing chromomagnetic field:

$$V(\vec{0}) = \frac{T}{\pi^2 R^2} \sum_{s,k} \frac{1}{J_1^2(\epsilon_k^0)} \int_{-\infty}^{+\infty} dk_z \ln |1 - e^{-\beta(\omega^0 + s\omega) + i\phi}|. \quad (\text{C10})$$

[1] N. Michael Davies, Timothy J. Hollowood, Valentin V. Khoze, and Michael P. Mattis, “Gluino condensate

and magnetic monopoles in supersymmetric gluodynamics”

ics,” *Nucl. Phys. B* **559**, 123–142 (1999), arXiv:hep-th/9905015.

[2] Erich Poppitz, Thomas Schäfer, and Mithat Unsal, “Continuity, Deconfinement, and (Super) Yang-Mills Theory,” *JHEP* **10**, 115 (2012), arXiv:1205.0290 [hep-th].

[3] Kyle Aitken, Aleksey Cherman, Erich Poppitz, and Lawrence G. Yaffe, “QCD on a small circle,” *Phys. Rev. D* **96**, 096022 (2017), arXiv:1707.08971 [hep-th].

[4] Alexander M. Polyakov, “Quark Confinement and Topology of Gauge Groups,” *Nucl. Phys. B* **120**, 429–458 (1977).

[5] Kenneth G. Wilson, “Confinement of Quarks,” *Phys. Rev. D* **10**, 2445–2459 (1974).

[6] Alexander M. Polyakov, “Thermal Properties of Gauge Fields and Quark Liberation,” *Phys. Lett. B* **72**, 477–480 (1978).

[7] G. Boyd, J. Engels, F. Karsch, E. Laermann, C. Legeland, M. Lutgemeier, and B. Petersson, “Thermodynamics of SU(3) lattice gauge theory,” *Nucl. Phys. B* **469**, 419–444 (1996), arXiv:hep-lat/9602007.

[8] P. Braun-Munzinger and J. Wambach, “The Phase Diagram of Strongly-Interacting Matter,” *Rev. Mod. Phys.* **81**, 1031–1050 (2009), arXiv:0801.4256 [hep-ph].

[9] Reinhard Alkofer, Christian S. Fischer, Felipe J. Llanes-Estrada, and Kai Schwenzer, “What the Infrared Behaviour of QCD Vertex Functions in Landau gauge can tell us about Confinement,” *Int. J. Mod. Phys. E* **16**, 2720–2732 (2007), arXiv:0705.4402 [hep-ph].

[10] Kenji Fukushima, “Chiral effective model with the Polyakov loop,” *Phys. Lett. B* **591**, 277–284 (2004), arXiv:hep-ph/0310121.

[11] G. S. Bali, F. Bruckmann, G. Endrodi, Z. Fodor, S. D. Katz, S. Krieg, A. Schafer, and K. K. Szabo, “The QCD phase diagram for external magnetic fields,” *JHEP* **02**, 044 (2012), arXiv:1111.4956 [hep-lat].

[12] Gergely Endrodi, “Critical point in the QCD phase diagram for extremely strong background magnetic fields,” *JHEP* **07**, 173 (2015), arXiv:1504.08280 [hep-lat].

[13] Raoul Gatto and Marco Ruggieri, “Deconfinement and Chiral Symmetry Restoration in a Strong Magnetic Background,” *Phys. Rev. D* **83**, 034016 (2011), arXiv:1012.1291 [hep-ph].

[14] Christian S. Fischer, Jan Luecker, and Jens A. Mueller, “Chiral and deconfinement phase transitions of two-flavour QCD at finite temperature and chemical potential,” *Phys. Lett. B* **702**, 438–441 (2011), arXiv:1104.1564 [hep-ph].

[15] Wei-jie Fu, Jan M. Pawłowski, and Fabian Rennecke, “QCD phase structure at finite temperature and density,” *Phys. Rev. D* **101**, 054032 (2020), arXiv:1909.02991 [hep-ph].

[16] Kenji Fukushima, “Phase diagrams in the three-flavor Nambu-Jona-Lasinio model with the Polyakov loop,” *Phys. Rev. D* **77**, 114028 (2008), [Erratum: *Phys. Rev. D* 78, 039902 (2008)], arXiv:0803.3318 [hep-ph].

[17] L. Adamczyk et al. (STAR), “Global Λ hyperon polarization in nuclear collisions: evidence for the most vortical fluid,” *Nature* **548**, 62–65 (2017), arXiv:1701.06657 [nucl-ex].

[18] Kenji Fukushima, “Extreme matter in electromagnetic fields and rotation,” *Prog. Part. Nucl. Phys.* **107**, 167–199 (2019), arXiv:1812.08886 [hep-ph].

[19] Francesco Becattini and Michael A. Lisa, “Polarization and Vorticity in the Quark–Gluon Plasma,” *Ann. Rev. Nucl. Part. Sci.* **70**, 395–423 (2020), arXiv:2003.03640 [nucl-ex].

[20] Xu-Guang Huang, Jinfeng Liao, Qun Wang, and Xiaoliang Xia, “Vorticity and Spin Polarization in Heavy Ion Collisions: Transport Models,” *Lect. Notes Phys.* **987**, 281–308 (2021), arXiv:2010.08937 [nucl-th].

[21] Puyuan Bai and Lianyi He, “Absence of charged pion condensation in a magnetic field with parallel rotation,” (2025), arXiv:2512.07473 [nucl-th].

[22] Tao Guo, Jianing Li, Chengfu Mu, and Lianyi He, “Formation of a supergiant quantum vortex in a relativistic Bose-Einstein condensate driven by rotation and a parallel magnetic field,” *Phys. Rev. D* **106**, 094010 (2022), arXiv:2111.13159 [nucl-th].

[23] E. Siri and N. Sadooghi, “Thermodynamic properties of a relativistic Bose gas under rigid rotation,” *Phys. Rev. D* **110**, 036016 (2024), arXiv:2405.09481 [hep-ph].

[24] Alejandro Ayala, L. A. Hernández, K. Raya, and R. Zamora, “Fermion propagator in a rotating environment,” *Phys. Rev. D* **103**, 076021 (2021), [Erratum: *Phys. Rev. D* 104, 039901 (2021)], arXiv:2102.03476 [hep-ph].

[25] Hao-Lei Chen, Kenji Fukushima, Xu-Guang Huang, and Kazuya Mameda, “Analogy between rotation and density for Dirac fermions in a magnetic field,” *Phys. Rev. D* **93**, 104052 (2016), arXiv:1512.08974 [hep-ph].

[26] Yin Jiang and Jinfeng Liao, “Pairing Phase Transitions of Matter under Rotation,” *Phys. Rev. Lett.* **117**, 192302 (2016), arXiv:1606.03808 [hep-ph].

[27] Irving I. Gaspar, Luis A. Hernández, and Renato Zamora, “Chiral symmetry restoration in a rotating medium,” *Phys. Rev. D* **108**, 094020 (2023), arXiv:2305.00101 [hep-ph].

[28] Tian Xu and Yin Jiang, “Proca equation and vector field quantization in a rotating system,” *Chin. Phys. C* **45**, 114102 (2021), arXiv:2106.04851 [hep-th].

[29] Minghua Wei and Mei Huang, “Spin alignment of vector mesons from quark dynamics in a rotating medium*,” *Chin. Phys. C* **47**, 104105 (2023), arXiv:2303.01897 [hep-ph].

[30] Aage Bohr, “Rotational motion in nuclei,” *Rev. Mod. Phys.* **48**, 365–374 (1976).

[31] Takaharu Otsuka, Yusuke Tsunoda, Takashi Abe, Noritaka Shimizu, and Piet Van Duppen, “Underlying structure of collective bands and self-organization in quantum systems,” *Phys. Rev. Lett.* **123**, 222502 (2019), arXiv:1907.10759 [nucl-th].

[32] A. Vilenkin, “Parity Violating Currents in Thermal Radiation,” *Phys. Lett. B* **80**, 150–152 (1978).

[33] A. Vilenkin, “MACROSCOPIC PARITY VIOLATING EFFECTS: NEUTRINO FLUXES FROM ROTATING BLACK HOLES AND IN ROTATING THERMAL RADIATION,” *Phys. Rev. D* **20**, 1807–1812 (1979).

[34] A. Vilenkin, “QUANTUM FIELD THEORY AT FINITE TEMPERATURE IN A ROTATING SYSTEM,” *Phys. Rev. D* **21**, 2260–2269 (1980).

[35] Dam T. Son and Piotr Surowka, “Hydrodynamics with Triangle Anomalies,” *Phys. Rev. Lett.* **103**, 191601 (2009), arXiv:0906.5044 [hep-th].

[36] Shu Ebihara, Kenji Fukushima, and Kazuya Mameda, “Boundary effects and gapped dispersion in rotating fermionic matter,” *Phys. Lett. B* **764**, 94–99 (2017), arXiv:1608.00336 [hep-ph].

[37] M. N. Chernodub and Shinya Gongyo, “Interacting

fermions in rotation: chiral symmetry restoration, moment of inertia and thermodynamics,” *JHEP* **01**, 136 (2017), arXiv:1611.02598 [hep-th].

[38] M. N. Chernodub and Shinya Gongyo, “Effects of rotation and boundaries on chiral symmetry breaking of relativistic fermions,” *Phys. Rev. D* **95**, 096006 (2017), arXiv:1702.08266 [hep-th].

[39] Xinyang Wang, Minghua Wei, Zhibin Li, and Mei Huang, “Quark matter under rotation in the NJL model with vector interaction,” *Phys. Rev. D* **99**, 016018 (2019), arXiv:1808.01931 [hep-ph].

[40] Yidian Chen, Danning Li, and Mei Huang, “Inhomogeneous chiral condensation under rotation in the holographic QCD,” *Phys. Rev. D* **106**, 106002 (2022), arXiv:2208.05668 [hep-ph].

[41] Yuki Fujimoto, Kenji Fukushima, and Yoshimasa Hidaka, “Deconfining Phase Boundary of Rapidly Rotating Hot and Dense Matter and Analysis of Moment of Inertia,” *Phys. Lett. B* **816**, 136184 (2021), arXiv:2101.09173 [hep-ph].

[42] V. V. Braguta, A. Yu. Kotov, D. D. Kuznedelev, and A. A. Roenko, “Study of the Confinement/Deconfinement Phase Transition in Rotating Lattice SU(3) Gluodynamics,” *Pisma Zh. Eksp. Teor. Fiz.* **112**, 9–16 (2020).

[43] V. V. Braguta, A. Yu. Kotov, D. D. Kuznedelev, and A. A. Roenko, “Influence of relativistic rotation on the confinement-deconfinement transition in gluodynamics,” *Phys. Rev. D* **103**, 094515 (2021), arXiv:2102.05084 [hep-lat].

[44] Xun Chen, Lin Zhang, Danning Li, Defu Hou, and Mei Huang, “Gluodynamics and deconfinement phase transition under rotation from holography,” *JHEP* **07**, 132 (2021), arXiv:2010.14478 [hep-ph].

[45] M. N. Chernodub, “Inhomogeneous confining-deconfining phases in rotating plasmas,” *Phys. Rev. D* **103**, 054027 (2021), arXiv:2012.04924 [hep-ph].

[46] Yin Jiang, “Rotating SU(2) gluon matter and deconfinement at finite temperature,” *Phys. Lett. B* **853**, 138655 (2024), arXiv:2312.06166 [hep-th].

[47] Yin Jiang, “Inhomogeneous SU(2) gluon matter under rotation,” *Phys. Rev. D* **110**, 054047 (2024), arXiv:2406.03311 [nucl-th].

[48] Fei Sun, Jingdong Shao, Rui Wen, Kun Xu, and Mei Huang, “Chiral phase transition and spin alignment of vector mesons in the polarized-Polyakov-loop Nambu–Jona-Lasinio model under rotation,” *Phys. Rev. D* **109**, 116017 (2024), arXiv:2402.16595 [hep-ph].

[49] Yidian Chen, Xun Chen, Danning Li, and Mei Huang, “Deconfinement and chiral restoration phase transition under rotation from holography in an anisotropic gravitational background,” *Phys. Rev. D* **111**, 046006 (2025), arXiv:2405.06386 [hep-ph].

[50] Sheng Wang, Jun-Xia Chen, Defu Hou, and Hai-Cang Ren, “Strong Coupling Expansion of Gluodynamics on a Lattice under Rotation,” (2025), arXiv:2505.15487 [hep-ph].

[51] Kenji Fukushima and Yusuke Shimada, “Imaginary rotating gluonic matter at strong coupling,” *Phys. Lett. B* **868**, 139716 (2025), arXiv:2506.03560 [hep-ph].

[52] David J. Gross, Robert D. Pisarski, and Laurence G. Yaffe, “QCD and Instantons at Finite Temperature,” *Rev. Mod. Phys.* **53**, 43 (1981).

[53] Nathan Weiss, “The Effective Potential for the Order Parameter of Gauge Theories at Finite Temperature,” *Phys. Rev. D* **24**, 475 (1981).

[54] Shi Chen, Kenji Fukushima, and Yusuke Shimada, “Perturbative Confinement in Thermal Yang-Mills Theories Induced by Imaginary Angular Velocity,” *Phys. Rev. Lett.* **129**, 242002 (2022), arXiv:2207.12665 [hep-ph].

[55] Sergei G. Matinyan and G. K. Savvidy, “Vacuum Polarization Induced by the Intense Gauge Field,” *Nucl. Phys. B* **134**, 539–545 (1978).

[56] G. K. Savvidy, “Infrared Instability of the Vacuum State of Gauge Theories and Asymptotic Freedom,” *Phys. Lett. B* **71**, 133–134 (1977).

[57] N. K. Nielsen and P. Olesen, “An Unstable Yang-Mills Field Mode,” *Nucl. Phys. B* **144**, 376–396 (1978).

[58] Peter N. Meisinger and Michael C. Ogilvie, “Finite temperature quark confinement,” *Phys. Lett. B* **407**, 297–302 (1997), arXiv:hep-lat/9703009.

[59] Howard E. Haber and H. Arthur Weldon, “On the Relativistic Bose-einstein Integrals,” *J. Math. Phys.* **23**, 1852 (1982).

[60] Howard E. Haber and H. Arthur Weldon, “Finite Temperature Symmetry Breaking as Bose-Einstein Condensation,” *Phys. Rev. D* **25**, 502 (1982).

[61] A. Actor, “Zeta Function Regularization of High Temperature Expansions in Field Theory,” *Nucl. Phys. B* **265**, 689–719 (1986).

[62] A. Actor, “More on Zeta Function Regularization of High Temperature Expansions,” *Fortsch. Phys.* **35**, 793–829 (1987).

[63] Peter N. Meisinger and Michael C. Ogilvie, “The Finite temperature SU(2) Savvidy model with a nontrivial Polyakov loop,” *Phys. Rev. D* **66**, 105006 (2002), arXiv:hep-ph/0206181.

[64] D. Kay, A. Kumar, and Ragavachari Parthasarathy, “Savvidy vacuum in SU(2) Yang-Mills theory,” *Mod. Phys. Lett. A* **20**, 1655–1662 (2005).

[65] R. Parthasarathy and Alok Kumar, “SU(2) Yang-Mills theory in Savvidy background at finite temperature and chemical potential,” *Phys. Rev. D* **75**, 085007 (2007), arXiv:hep-th/0609090.

[66] J. Engels, F. Karsch, and K. Redlich, “Scaling properties of the energy density in SU(2) lattice gauge theory,” *Nucl. Phys. B* **435**, 295–310 (1995), arXiv:hep-lat/9408009.

[67] Jens Braun, Holger Gies, and Jan M. Pawłowski, “Quark Confinement from Color Confinement,” *Phys. Lett. B* **684**, 262–267 (2010), arXiv:0708.2413 [hep-th].

[68] V. N. Gribov, “Quantization of Nonabelian Gauge Theories,” *Nucl. Phys. B* **139**, 1 (1978).

[69] Taichiro Kugo and Izumi Ojima, “Local Covariant Operator Formalism of Nonabelian Gauge Theories and Quark Confinement Problem,” *Prog. Theor. Phys. Suppl.* **66**, 1–130 (1979).

[70] Daniel Zwanziger, “Fundamental modular region, Boltzmann factor and area law in lattice gauge theory,” *Nucl. Phys. B* **412**, 657–730 (1994).

[71] M. N. Chernodub, V. A. Goy, and A. V. Molochkov, “Inhomogeneity of a rotating gluon plasma and the Tolman–Ehrenfest law in imaginary time: Lattice results for fast imaginary rotation,” *Phys. Rev. D* **107**, 114502 (2023), arXiv:2209.15534 [hep-lat].

[72] Paolo Cea, Leonardo Cosmai, and Massimo D’Elia, “QCD dynamics in a constant chromomagnetic field,” *JHEP* **12**, 097 (2007), arXiv:0707.1149 [hep-lat].

- [73] Haolei Chen and Xuguang Huang, “Chromomagnetic Condensate in Finite-Temperature $SU(2)$ Yang-Mills Theory under Imaginary Rotation,” arXiv on the same day (2026).
- [74] Hao-Lei Chen, Kenji Fukushima, Xu-Guang Huang, and Kazuya Mameda, “Surface Magnetic Catalysis,” *Phys. Rev. D* **96**, 054032 (2017), [arXiv:1707.09130 \[hep-ph\]](https://arxiv.org/abs/1707.09130).